Accepted Manuscript

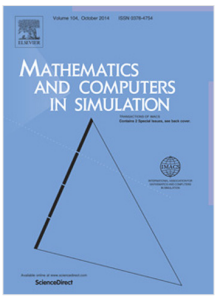

Induced magnetic field analysis for the peristaltic transport of non-Newtonian nanofluid in an annulus

Hina Sadaf, Muhammad Usman Akbar, S. Nadeem

PII: S0378-4754(18)30002-8
DOI: https://doi.org/10.1016/j.matcom.2017.12.009
Reference: MATCOM 4530

To appear in: *Mathematics and Computers in Simulation*

Received date : 7 April 2017
Revised date : 24 December 2017
Accepted date : 30 December 2017

Please cite this article as: H. Sadaf, M.U. Akbar, S. Nadeem, Induced magnetic field analysis for the peristaltic transport of non-Newtonian nanofluid in an annulus, *Math. Comput. Simulation* (2018), https://doi.org/10.1016/j.matcom.2017.12.009

Induced magnetic field analysis for the peristaltic transport of non-Newtonian nanofluid in an annulus

Hina Sadaf[1], *Muhammad Usman Akbar*[2], *S. Nadeem*[3]

[1] *DBS&H, CEME, National University of Sciences and Technology, Islamabad, Pakistan*

[2] *Department of Computer Engineering, Bahria University, Islamabad* 44000 *Pakistan*

[3] *Department of Mathematics, Quaid-i-Azam University* 45320, *Islamabad* 44000 *Pakistan*

Abstract: This paper examines the peristaltic flow of Williamson nanofluid in an annulus in the presence of induced magnetic field. Present problem is determined under the molds of long wavelength and low Reynolds number approximation. This theoretical problem can be considered as a mathematical illustration to the movement of fluids in the presence of an endoscope or catheter tube. The inner cylinder is rigid, whereas the outward cylinder proceeds a sinusoidal wave moving down its walls. The analytical solution is obtained by using Homotopy perturbation method. Mathematica numerical simulations are adopted to calculate frictional forces and pressure rise. Behavior of various physical parameters is presented through graphs. It is found that induced magnetic field and current density enhances by increasing value of magnetic Reynolds number. It is also found that temperature profile upturns with an upturn in Brownian motion and thermophoresis parameter.

Keywords: Peristaltic flow，heat transfer, induced magnetic field，Williamson nanofluid model, annulus, Homotopy perturbation method.

Introduction

Peristaltic motion of different fluids has attained a special position because of its wide applications such as the swallowing of food through the esophagus, sanitary fluids, corrosive fluids, locomotion of some warms and fluids in lymphatic vessels, etc. After the first analysis made by Latham [1], a lot of efforts have been made to study the peristaltic flow considering Newtonian as well as non-Newtonian fluids [2−16].

Now a days Nanofluid science has fascinated devotion of many investigators because such fluids enhance thermal conductivity of the base fluid. Nanofluid firstly presented by Choi [17] that was defined nanoparticles suspensions into base fluids, including small particles of length scale less than 100nm. These particles are generally a metal or metal oxide, increase conduction and convection coefficients, letting for more heat transfer out of the coolant. A comprehensive analysis of nanofluids was deliberated by Buongiorno [18]. The problem of boiling nanofluids on horizontal narrow tubes was visualized by Das et al. [19]. Nadeem et al. [20] examined nanoparticles analysis on peristaltic flow of Prandtl fluid model in the presence of an endoscopic tube. Kuznetsov and Nield [21] reported nanofluid past a rigid flat plate for natural convective boundary layer flow. Khan and Pop [22] analyzed two-dimensional boundary layer flow of nanofluid over an impermeable stretching sheet. Heat transfer improvement by consuming nanofluids in forced convection streams have been discussed by Marga et al. [23]. Rana and Bhargava [24] stretched the work of Khan and Pop for nonlinearly stretching sheet. The inspiration of endoscope tube on the peristaltic passage of nanofluid has been examined by Akbar and Nadeem [25]. Ellahi et al. [26] debated series solutions of non-Newtonian nanofluids for Vogel's and Reynolds' viscosity model by smearing homotopy analysis method.

Corresponding author email: hinasadaf46@yahoo.com

Induced magnetic field concept in peristalsis had been discovered by some of the researchers. Mekheimer [27] deliberated the consequence of an induced magnetic field on the peristaltic flow of a non-Newtonian fluid. Induced magnetic field impact on peristaltic flow in an annulus has been inspected by Abd elmaboud [28]. He discussed that his theoretical model may be considered as mathematical illustration to the movement of conductive physiological fluids in the presence of an endoscopic tube. Nadeem and Akram [29] presented the induced magnetic field effect on peristaltic flow of couple stress fluid in an asymmetric channel. Reddy et al. [30] examined the problem of peristaltic flow in an inclined symmetric channel filled with porous material under the long wavelength and low Reynolds number assumptions. They used perturbation expansion to analyze the problem and considering small Weissenberg number. Mekheimer et al. [31] discussed induced magnetic field impact on peristaltic flow of a magneto-micropolar fluid.

The Homotopy perturbation method, first proposed by Ji-Huan He [32, 33] for resolving differential and integral equations, linear and nonlinear, has been the topic of wide analytical and numerical studies. The method, which is a connection of the traditional perturbation method and homotopy in topology, distorts continuously to a simple problem which is easily solved. This method, which does not require a small parameter in an equation, has a important advantage in that delivers an analytical approximate solution to a extensive variety of linear and nonlinear problems in applied sciences. For more aspects see the Refs. [34-37].

The current problem is undertaken to study the effects of induced magnetic on the peristaltic flow of Williamson nanofluid in an annulus. Analytical solutions are accepted out with the aid of homotopy perturbation technique for velocity, temperature, nanoparticle concentration, axial induced magnetic field and for current density distribution. Graphical consequences for pressure rise, pressure gradient, friction forces, current density distribution, and the axial induced magnetic field has been designed for different values of the physical parameters arriving in the problem.

Model of the problem

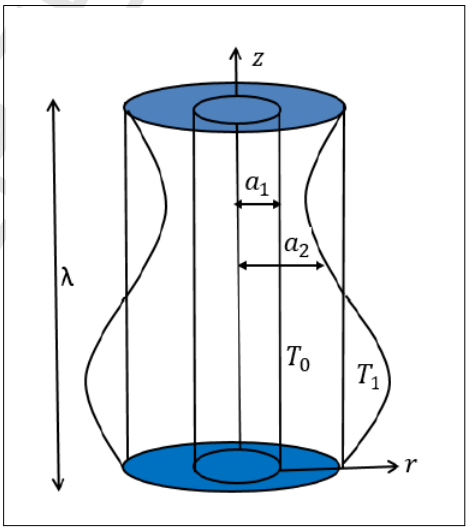

Fig. a, Geometry of the problem

Assume the hydro-magnetic flow of a nano Williamson, incompressible and electrically conducting fluid through the gap between two vertical cylinders. The inner cylinder is rigid retained at a temperature $\overline{T}_0$, while the outer cylinder has a sinusoidal wave traveling down its walls and retained at temperature $\overline{T}_1$. The system is stressed by an external radial uniform magnetic field of strength $\frac{\overline{H}_0\overline{R}_2}{\overline{R}}$ which will give grow to an induced magnetic field $\overline{H}^+(\overline{h}_{\overline{R}}(\overline{R},\overline{Z},\bar{t}),0,\overline{h}_{\overline{Z}}(\overline{R},\overline{Z},\bar{t}))$ and the total magnetic field will be $\overline{H}^+(\overline{h}_{\overline{R}}(\overline{R},\overline{Z},\bar{t})+\frac{\overline{H}_0\overline{R}_2}{\overline{R}},0,\overline{h}_{\overline{Z}}(\overline{R},\overline{Z},\bar{t}))$. The walls of the cylinders are expected to be non-conductive, and the wall surface geometry are defined as

$$\overline{R}_1 = a_1, \tag{1}$$

$$\overline{R}_2 = a_2 + b\sin\frac{2\pi}{\lambda}(\overline{Z} - c\bar{t}), \tag{2}$$

where a_1, a_2, λ, b, c, is the radius of the inner and outer cylinders, wavelength, wave amplitude, and wave speed respectively. Basic equations of hydro-magnetic flow of a Williamson nanofluid, avoiding the displacement currents and free charges, are
Maxwell's equations

$$\nabla.\overline{\mathbf{H}}^+ = 0,\ \nabla.\overline{\mathbf{E}}^+ = 0, \tag{3}$$

$$\nabla\times\overline{\mathbf{H}}^+ = \overline{\mathbf{J}},\ \text{where}\ \overline{\mathbf{J}} = \sigma\{\overline{\mathbf{E}} + \mu_e(\overline{\mathbf{V}}\times\overline{\mathbf{H}}^+)\}, \tag{4}$$

$$\nabla\times\overline{\mathbf{E}}^+ = -\mu_e\frac{\partial\overline{\mathbf{H}}^+}{\partial\bar{t}} \tag{5}$$

Continuity and Navier Stokes equations are

$$\operatorname{div}\overline{\mathbf{V}} = 0, \tag{6}$$

$$\rho_f\frac{d\overline{\mathbf{V}}}{d\bar{t}} = \operatorname{div}\overline{\mathbf{S}} + \rho_f\mathbf{f} + \mu_e(\overline{\mathbf{J}}\times\overline{\mathbf{H}}^+), \tag{7}$$

Combining Eqs. (3) to (5) we obtain induction equation

$$\frac{\partial\overline{\mathbf{H}}^+}{\partial\bar{t}} = \nabla\times\left\{\overline{\mathbf{V}}\times\overline{\mathbf{H}}^+\right\} + \zeta\nabla^2\overline{\mathbf{H}}^+. \tag{8}$$

We are using the Buongiorno [18] nanofluid model therefore the Nanoparticle temperature and concentration equations are shown as

$$\frac{d\overline{T}}{d\bar{t}} = \frac{k}{(\rho c)_f}\nabla^2\overline{T} + \frac{(\rho c)_p}{(\rho c)_f}[D_B\nabla\overline{C}.\nabla\overline{T} + (\frac{D_{\overline{T}}}{\overline{T}_1})\nabla\overline{T}.\nabla\overline{T}], \tag{9}$$

$$\frac{d\overline{C}}{d\bar{t}} = D_B\nabla^2\overline{C} + (\frac{D_{\overline{T}}}{\overline{T}_1})\nabla^2\overline{T}, \tag{10}$$

where $\overline{\mathbf{E}}^{+}$ is the induced electric field, $\overline{\mathbf{J}}$ is the electric current density, σ is the electrical conductivity, μ_e is the magnetic permeability, $\zeta = \frac{1}{\sigma\mu_e}$ denotes the magnetic diffusivity, $\overline{\mathbf{V}}$ is the velocity component, $\overline{\mathbf{S}}$ gives the Cauchy stress tensor, $\overline{C}$ is the nanoparticle concentration, D_B the Brownian diffusion coefficients of mass diffusivity and $D_{\overline{T}}$ the thermophoretic diffusion coefficient respectively. $\tau_1 = \frac{(\rho c)_p}{(\rho c)_f}$ depicts the ratio of the effective heat capacity in the case of nanoparticle material and heat capacity of the fluid. The expression of Cauchy stress tensor is defined [38] as

$$\overline{\mathbf{S}} = -\overline{P}\mathbf{I} + \overline{\boldsymbol{\tau}}, \tag{11}$$

$$\overline{\boldsymbol{\tau}} = [[\eta_\infty + (\eta_{0+}\eta_\infty)(1-\Gamma\overline{\dot{\gamma}})^{-1}]\overline{\dot{\gamma}_i}], \tag{12}$$

in which $\overline{\boldsymbol{\tau}}$, η_0, η_∞, Γ, defines extra stress tensor, zero shear rate viscosity, infinite rate of shear viscosity, time constant respectively and $\overline{\dot{\gamma}}$ now defined as

$$\overline{\dot{\gamma}} = \sqrt{\frac{1}{2}\sum_i\sum_j \overline{\dot{\gamma}}_{ij}\,\overline{\dot{\gamma}}_{ji}} = \sqrt{\frac{1}{2}\boldsymbol{\pi}}, \tag{13}$$

where

$$\boldsymbol{\pi} = trace(\operatorname{grad}\overline{\mathbf{A}} + (\operatorname{grad}\overline{\mathbf{A}})^T)^2, \tag{14}$$

in which π define second invariant strain tensor. We assume in the Eq. (12) the case for which we take $\eta_\infty = 0$ and $\Gamma\overline{\dot{\gamma}} < 1$ thus we can write

$$\overline{\boldsymbol{\tau}} = \eta_0[(1+\Gamma\overline{\dot{\gamma}})]\overline{\dot{\gamma}_i}, \tag{15}$$

$$\overline{\dot{\gamma}_i} = \mathbf{L} + \mathbf{L}^T, \tag{16}$$

where η_∞, η_0 and Γ define infinite shear rate viscosity, zero shear rate viscosity and time constant respectively. In the fixed coordinate $(\overline{R},\ \overline{Z})$, the flow in the cylinders is unsteady, it converts into steady flow in a wave frame $(\overline{r},\overline{z})$ traveling with same speed as the wave travels in the $\overline{Z}$ directions. The conversions between the wave frames of reference are

$$\overline{r} = \overline{R},\ \overline{z} = \overline{Z} - c\overline{t},\ \overline{w} = \overline{W} - c,\ \overline{u} = \overline{U}. \tag{17}$$

In the wave frame $\overline{u}$ and $\overline{w}$ denote the velocity mechanisms. The boundary limits are expressed as

$$\overline{w} = -c, \text{ at } \bar{r} = \bar{r}_1, \text{ and } \overline{w} = -c \text{ at } \bar{r} = \bar{r}_2 = a_2 + b\sin\frac{2\pi}{\lambda}(\bar{z}),$$
$$\overline{T} = \overline{T}_0 \text{ at } \bar{r} = \bar{r}_1, \text{ and } \overline{T} = \overline{T}_1 \text{ at } \bar{r} = \bar{r}_2,$$
$$\overline{C} = \overline{C}_0 \text{ at } \bar{r} = \bar{r}_1, \text{ and } \overline{C} = \overline{C}_1 \text{ at } \bar{r} = \bar{r}_2. \qquad (18)$$

in the above equations $D_{\bar{T}}$ the thermophoretic diffusion coefficient and D_B the Brownian diffusion coefficients of mass diffusivity.
Introducing the dimensionless variables

$$R = \frac{\overline{R}}{a_2},\ r = \frac{\bar{r}}{a_2},\ W = \frac{\overline{W}}{c},\ w = \frac{\overline{w}}{c},\ Z = \frac{\overline{Z}}{\lambda},\ z = \frac{\bar{z}}{\lambda},\ U = \frac{\lambda\overline{U}}{ca_2},$$
$$u = \frac{\lambda\bar{u}}{a_2 c},\ t = \frac{c\bar{t}}{\lambda},\ P = \frac{a_2^2\overline{P}}{c\lambda\eta},\ \theta = \frac{\overline{T} - \overline{T}_1}{\overline{T}_0 - \overline{T}_1},\ \hat{\delta} = \frac{a_2}{\lambda},\ \mathrm{Re} = \frac{\rho_f c a_2}{\eta},$$
$$S = \frac{a_2\overline{S}}{c\eta},\ r_1 = \frac{\bar{r}_1}{a_2} = \frac{a_1}{a_2} = \varepsilon,\ r_2 = \frac{\bar{r}_2}{a_2} = 1 + \phi\sin 2\pi z,\ We = \frac{\Gamma c}{a_2},$$
$$\alpha_f = \frac{k}{(\rho c)f},\ N_b = \frac{(\rho c)_p D_B(\overline{C}_0 - \overline{C}_1)}{\alpha_f(\rho c)_f},\ N_t = \frac{(\rho c)_p D_{\bar{T}}(\overline{T}_0 - \overline{T}_1)}{\overline{T}_1\alpha_f(\rho c)_f},$$
$$G_r = \frac{\rho_f g\alpha_{\bar{T}} a_2^2(\overline{T}_0 - \overline{T}_1)}{\eta c},\ B_r = \frac{\rho_f g\alpha_{\bar{C}} a_2^2(\overline{C}_0 - \overline{C}_1)}{\eta c},\ \phi = \frac{b}{a_2},\ \tau = \frac{\bar{\tau}a_2}{\eta c}$$
$$\dot{\gamma} = \frac{a_2}{c}\bar{\dot{\gamma}},\ \sigma = \frac{\overline{C} - \overline{C}_1}{\overline{C}_0 - \overline{C}_1},\ h_r = \frac{\overline{h}_r}{H_0},\ h_z = \frac{\overline{h}_z}{H_0}. \qquad (19)$$

We define N_t, Re, B_r, G_r, We, N_b, $\hat{\delta}$, ϕ ‹ 1, $\alpha_{\bar{T}}$, $\alpha_{\bar{c}}$, are the thermophoresis parameter, Reynolds number, local nanoparticle Grashof number, local temperature Grashof number, Weissenberg number, Brownian motion parameter, wave number, ϕ is the amplitude ratio, coefficient of thermal expansion, coefficient of expansion with nano concentration respectively.
Using Eqs. (17) and (19) into Eqs. (1) to (10), we obtain

$$\frac{\partial h_r}{\partial r} + \frac{h_r}{r} + \hat{\delta}\frac{\partial h_z}{\partial z} = 0, \qquad (20)$$
$$\frac{\partial u}{\partial r} + \frac{u}{r} + \frac{\partial w}{\partial z} = 0, \qquad (21)$$
$$\hat{\delta}^3\,\mathrm{Re}\left(u\frac{\partial u}{\partial r} + w\frac{\partial u}{\partial z}\right) = -\frac{\partial p}{\partial r} + \hat{\delta}^2\frac{\partial}{\partial z}(\boldsymbol{\tau}_{rz}) + \frac{\hat{\delta}}{r}\frac{\partial}{\partial r}(r\boldsymbol{\tau}_{rr}) - \frac{\hat{\delta}}{r}\boldsymbol{\tau}_{\theta\theta} + S^2\,\mathrm{Re}\,\hat{\delta}\left[\hat{\delta}\left(\frac{1}{r}\frac{\partial r_2}{\partial z} + \frac{\partial h_r}{\partial z}\right) - \frac{\partial h_z}{\partial r}\right]h_z, \qquad (22)$$

$$\hat{\delta}\,\mathrm{Re}\left(u\frac{\partial w}{\partial r}+w\frac{\partial w}{\partial z}\right)=-\frac{\partial p}{\partial z}+\frac{1}{r}\frac{\partial}{\partial r}(r\boldsymbol{\tau}_{rz})+\hat{\delta}\frac{\partial}{\partial r}(\boldsymbol{\tau}_{zz})+S^2\,\mathrm{Re}\left[\frac{\partial h_z}{\partial r}-\hat{\delta}\left(\frac{1}{r}\frac{\partial r_2}{\partial z}+\frac{\partial h_r}{\partial z}\right)\right]$$
$$\left(\frac{r_2}{r}+h_r\right)+G_r\theta+B_r\sigma, \tag{23}$$

$$\hat{\delta}\left\{\left[u\frac{\partial}{\partial r}+w\frac{\partial}{\partial z}-\frac{\partial u}{\partial r}\right]\left(\frac{r_2}{r}+h_r\right)-\hat{\delta}h_z\frac{\partial u}{\partial z}\right\}=\frac{\hat{\delta}}{R_m}\frac{\partial}{\partial z}\left(\hat{\delta}\left(\frac{1}{r}\frac{\partial r_2}{\partial z}+\frac{\partial h_r}{\partial z}\right)-\frac{\partial h_z}{\partial r}\right), \tag{24}$$

$$\hat{\delta}\left[u\frac{\partial h_z}{\partial r}+w\frac{\partial h_z}{\partial z}-h_z\frac{\partial w}{\partial z}\right]-\left(\frac{r_2}{r}+h_r\right)\frac{\partial w}{\partial r}=\frac{1}{R_m}\left[\frac{1}{r}\frac{\partial}{\partial r}\left(r\frac{\partial h_z}{\partial r}\right)-\hat{\delta}\frac{\partial}{\partial z}\left(\left(\frac{\partial}{\partial r}+\frac{1}{r}\right)\left(\frac{r_2}{r}+h_r\right)\right)\right], \tag{25}$$

$$\frac{1}{r}\frac{\partial}{\partial r}\left(r\frac{\partial\theta}{\partial r}\right)+N_b\frac{\partial\theta}{\partial r}\frac{\partial\sigma}{\partial r}+N_t\left(\frac{\partial\theta}{\partial r}\right)^2=0, \tag{26}$$

$$\frac{1}{r}\frac{\partial}{\partial r}\left(r\frac{\partial\sigma}{\partial r}\right)+\frac{N_t}{N_b}\left(\frac{1}{r}\frac{\partial}{\partial r}\left(r\frac{\partial\theta}{\partial r}\right)\right)=0. \tag{27}$$

where

We note above equations are non-linear，therefore，we are involved to solve our problem by the suppositions of low Reynolds number and long wavelength，avoiding the terms of order $\hat{\delta}$ and greater，Eqs. (20) to (27) take the following form

$$\frac{\partial h_r}{\partial r}+\frac{h_r}{r}=0 \tag{28}$$

$$\frac{\partial p}{\partial r}=0, \tag{29}$$

$$\frac{\partial p}{\partial z}=\frac{1}{r}\frac{\partial}{\partial r}\left(r\left(1+We\frac{\partial w}{\partial r}\right)\left(\frac{\partial w}{\partial r}\right)\right)+S^2\,\mathrm{Re}\frac{\partial h_z}{\partial r}\left(\frac{r_2}{r}+h_r\right)+G_r\theta+B_r\sigma, \tag{30}$$

$$\left(\frac{r_2}{r}+h_r\right)\frac{\partial w}{\partial r}=-\frac{1}{R_m}\left[\frac{1}{r}\frac{\partial}{\partial r}\left(r\frac{\partial h_z}{\partial r}\right)\right], \tag{31}$$

$$\frac{1}{r}\frac{\partial}{\partial r}\left(r\frac{\partial\theta}{\partial r}\right)+N_b\frac{\partial\sigma}{\partial r}\frac{\partial\theta}{\partial r}+N_t\left(\frac{\partial\theta}{\partial r}\right)^2=0, \tag{32}$$

$$\frac{1}{r}\frac{\partial}{\partial r}\left(r\frac{\partial\sigma}{\partial r}\right)+\frac{N_t}{N_b}\left(\frac{1}{r}\frac{\partial}{\partial r}\left(r\frac{\partial\theta}{\partial r}\right)\right)=0, \tag{33}$$

where

$S^2=\frac{H_0^2\mu_e}{\rho c^2}$ and $R_m=\frac{a_2 c}{\zeta}$ are the Strommers number (magnetic force number) and the magnetic Reynolds number respectively. Eq. (29) illustrates that p is not a function of r. The final dimensionless boundary limits for non-conductive cylinders are

$$w=-1\,\text{at}\,r=r_1,\ w=-1,\ h_r=h_z=0,\ \text{at}\,r=r_2,$$
$$\sigma=\theta=1\,\text{at}\,r=r_1,\ \sigma=\theta=0\,\text{at}\,r=r_2, \tag{34}$$

Analytical solutions

Homotopy perturbation solution

Solution of Eq. (31) subject to the relevant boundary condition shows that $h_r = 0$. (i.e continuity of the normal component of the magnetic field across the boundary gives that induced magnetic field in the radial direction is zero). Integrating Eq. (31) after replacing $h_r = 0$ one finds

$$\frac{\partial h_z}{\partial r} = -\left(\frac{R_m r_2}{r}\right) w - \frac{x_1}{r}. \tag{35}$$

To determine the constant x_1, we find from Eqs. (4) and (35) as

$$J_\theta = -\frac{\partial h_z}{\partial r} = \left(\frac{R_m r_2}{r}\right) w + \frac{x_1}{r}. \tag{36}$$

Since $J_\theta = 0$ at $r = r_2$ so $x_1 = R_m r_2$. Now replace $h_r = 0$ and eliminate $\frac{\partial h_z}{\partial r}$ in Eq. (30). To achieve the solution of above equations, we have used homotopy perturbation method. The homotopy perturbation technique allows [39, 40] to write Eqs. (30), (32), and (33) as

$$H(j,\sigma) = (1-j)\left[£(\sigma) - £(\sigma_{20})\right] + j\left[£(\sigma) + \frac{N_t}{N_b}\left(\frac{1}{r}\frac{\partial}{\partial r}\left(r\frac{\partial \theta}{\partial r}\right)\right)\right], \tag{37}$$

$$H(j,\theta) = (1-j)[£(\theta) - £(\theta_{20})] + j\left[£(\theta) + N_t\left(\frac{\partial \theta}{\partial r}\right)^2 + N_b \frac{\partial \theta}{\partial r}\frac{\partial \sigma}{\partial r}\right], \tag{38}$$

$$H(j,w) = (1-j)\left[£(w) - £(w_{20})\right] + j\left[£(w) - \frac{\partial p}{\partial z} + \frac{1}{r}\frac{\partial}{\partial r}\left(rWe\left(\frac{\partial w}{\partial r}\right)^2\right) - \frac{M^2 r_2^2}{r^2} + G_r\theta + B_r\sigma\right], \tag{39}$$

where $M = S^2 \operatorname{Re} R_m$ (Hartmann number), $H = Mr_2$, and the linear operator and the initial predicts are selected as

$$\begin{aligned} £_{\theta r} &= £_{\sigma r} = \frac{1}{r}\frac{\partial}{\partial r}\left(r\frac{\partial}{\partial r}\right),\ £_{wr} = \frac{1}{r}\frac{\partial}{\partial r}\left(r\frac{\partial}{\partial r}\right) - \frac{M^2 r_2^2}{r^2}, \\ \sigma_{20}(r,z) &= \left(\frac{r-r_2}{r_1-r_2}\right),\ \theta_{20}(r,z) = \left(\frac{r-r_2}{r_1-r_2}\right), \\ w_{20} &= -1 + \frac{dp_0}{dz}\left(a_{11}r^2 + a_{12}r^H + a_{13}r^{-H}\right). \end{aligned} \tag{40}$$

Allowing to HPM, we describe

$$\theta = \theta_0 + j\theta_1 + j^2\theta_2 + ...,$$
$$\sigma = \sigma_0 + j\sigma_1 + j^2\sigma_2 + ...,$$
$$w = w_0 + jw_1 + j^2w_2 + ...,$$
$$F_i = F_{oi} + jF_{1i} + j^2F_{2i} + ..., \quad (41)$$

With the aid of above equations, Eqs. (37) to (39) after gathering the like powers of j and concluding the perturbation outcomes for parameter $j \to 1$, the appearance for concentration field, temperature and velocity can be printed as

$$\sigma = \ell_{28}r^2 + r\ell_{36} + \ell_{37}\ln r + \ell_{38}, \quad (42)$$

$$\theta = \ell_{39}r^3 + r^2\ell_{46} + \ell_{41}r + \ell_{47}\ln r + \ell_{48}, \quad (43)$$

The solutions of axial velocity and the axial induced magnetic field can be directly defined as

$$\begin{aligned} w = -1 + \frac{dp}{dz}\left(a_{11}r^2 + a_{12}r^H + a_{13}r^{-H}\right) + \left(-\frac{a_{21}}{r} + a_{27}r^2 - a_{22}r^3 + a_{23}r^{-1-2H}\right. \\ + a_{24}r^{1-H} + a_{25}r^{1+H} + a_{26}r^{-1+2H} + a_{28}r^H + a_{29}r^{-H}\Big) + \Big(\frac{a_{47}}{r} + a_{48}r^3 \\ + a_{49}r^4 + a_{50}r^{-2-3H} + a_{51}r^{-1-2H} + a_{52}r^{-2H} + a_{53}r^{-2-H} + a_{54}r^{1-H} + a_{55}r^{-2+H} \\ + a_{56}r^{1+H} + a_{57}r^{2-H} + a_{58}r^{2+H} + a_{59}r^{-1+2H} + a_{60}r^{2H} + a_{61}r^{-2+3H} + a_{62}r^2\ln r \\ + a_{63}r^2 + a_{64}r^H + a_{65}r^{-H}\Big). \end{aligned} \quad (44)$$

$$\begin{aligned} hz = \frac{-a_{21}r_2R_m}{r} + \frac{a_{47}r_2R_m}{r} - \frac{1}{2}a_{27}r^2r_2R_m + \frac{1}{4}a_{62}r^2r_2R_m - \frac{1}{2}a_{63}r^2r_2R_m \\ + \frac{1}{3}a_{22}r^3r_2R_m - \frac{1}{3}a_{48}r^3r_2R_m - \frac{1}{4}a_{49}r^4r_2R_m + \frac{a_{50}r^{-2-3H}r_2R_m}{2+3H} \\ + \frac{a_{53}r^{-2-H}r_2R_m}{H+2} + \frac{a_{24}r^{1-H}r_2R_m}{H-1} + \frac{a_{54}r^{1-H}r_2R_m}{H-1} - \frac{a_{57}r^{2-H}r_2R_m}{-H+2} \\ - \frac{a_{55}r^{-2+H}r_2R_m}{-2+H} + \frac{a_{52}r^{-2H}r_2R_m}{2H} + \frac{a_{29}r^{-H}r_2R_m}{H} + \frac{a_{65}r^{-H}r_2R_m}{H} \\ - \frac{a_{28}r^Hr_2R_m}{H} - \frac{a_{64}r^Hr_2R_m}{H} - \frac{a_{60}r^{2H}r_2R_m}{2H} - \frac{a_{25}r^{1+H}r_2R_m}{1+H} \\ - \frac{a_{56}r^{1+H}r_2R_m}{1+H} - \frac{a_{58}r^{2+H}r_2R_m}{2+H} - \frac{a_{61}r^{-2+3H}r_2R_m}{-2+3H} + \frac{a_{26}r^{2H}r_2R_m}{r-2Hr} \\ + \frac{a_{59}r^{2H}r_2R_m}{r-2Hr} + \frac{a_{23}r^{-2H}r_2R_m}{r+2Hr} + \frac{a_{51}r^{-2H}r_2R_m}{r+2Hr} - \frac{1}{2}a_{11}r^2r_2R_m\frac{dp}{dz} \\ + \frac{a_{13}r^{-H}r_2R_m}{H}\frac{dp}{dz} - \frac{a_{12}r^Hr_2R_m}{H}\frac{dp}{dz} - \frac{1}{2}a_{62}r^2r_2R_m\ln r - a_{71}. \end{aligned} \quad (45)$$

Current density distribution takes the following form

$$J_\theta = \frac{r_2 R_m}{r}(-1+\frac{dp}{dz}\left(a_{11}r^2 + a_{12}r^H + a_{13}r^{-H}\right)+(-\frac{a_{21}}{r}+a_{27}r^2 - a_{22}r^3$$
$$+a_{23}r^{-1-2H} + a_{24}r^{1-H} + a_{25}r^{1+H} + a_{26}r^{-1+2H} + a_{28}r^H + a_{29}r^{-H})$$
$$+(\frac{a_{47}}{r}+a_{48}r^3 + a_{49}r^4 + a_{50}r^{-2-3H} + a_{51}r^{-1-2H} + a_{52}r^{-2H} + a_{53}r^{-2-H}$$
$$+a_{54}r^{1-H} + a_{55}r^{-2+H} + a_{56}r^{1+H} + a_{57}r^{2-H} + a_{58}r^{2+H} + a_{59}r^{-1+2H}$$
$$+a_{60}r^{2H} + a_{61}r^{-2+3H} + a_{62}r^2\ln r + a_{63}r^2 + a_{64}r^H + a_{65}r^{-H}))+\frac{r_2 R_m}{r}, \quad (46)$$

in which all g_{ij} and a_{ij} are shown in appendix. Pressure gradient expression can be written as

$$\frac{dp}{dz} = \frac{F_i - a_{66} - a_{69} - a_{70}}{a_{67}}. \quad (47)$$

Dimensionless flow rate is defined as [41]

$$Q = F_i + \frac{1}{2}\left(1+\frac{\phi^2}{2}-\varepsilon^2\right). \quad (48)$$

The dimensionless expressions for time mean flow rate F_i, Pressure rise Δp and friction forces (at the wall) are defined as

$$\Delta p = \int_0^1 (\frac{dp}{dz})dz,\ F^0 = \int_0^1 -r_1^2(\frac{dp}{dz})dz,\ F^1 = \int_0^1 -r_2^2(\frac{dp}{dz})dz. \quad (49)$$

The relations for velocities, stream function and magnetic force function relation are defined as

$$w = \frac{1}{r}(\frac{\partial\Psi}{\partial r}),\ u = \frac{-1}{r}(\frac{\partial\Psi}{\partial z}),\ h_r = \frac{-1}{r}(\frac{\partial\phi}{\partial z}),\ h_z = \frac{1}{r}(\frac{\partial\phi}{\partial r}). \quad (50)$$

Making use of Eq. (44) and (45) into Eq · (49), we get stream function and magnetic force function, whereas all the constants are defined in an appendix and constants a_{28}, a_{29} and a_{64}, a_{65} appears when we solve Ist and 2nd iteration that can be evaluated by using Mathematica.

Graphical Results

In this unit axial induced magnetic field, current density distribution, temperature and nanoparticle concentration field, pressure rise, inner and outer friction forces, pressure gradient and stream lines are discussed. Figures. (1) to (23) is presented for this purpose. Inner and outer friction forces and pressure rise Δp are calculated numerically. Table 1 is plotted to see the validation of the applied homotopy technique. This method is shown that velocity profile satisfied Eq. 34 (boundary conditions of the problem) as well as Eq. 30 and the error generated in this process can be seen in the last column of Table 1. This technique is exposed a good validation for this problem with fixed parameters. Fig. 1, is designed to see the impact of velocity profile for Newtonian fluid as well non-Newtonian fluid. It is depicted in this plot,

velocity profile near the endoscopic or catheter tube decreases whereas quite opposite behavior is depicted near the peristaltic wall.

The axial induced magnetic field hz for diverse values of thermophoresis parameter, Brownian motion parameter and magnetic Reynolds number are depicted in the Figures. (2) to (4). In Fig. (2) and (3) it is seen that the axial induced magnetic field h_z drops by swelling the values of N_t and upsurges by swelling the values of N_b in the region $0.10 \le r \le 0.46$ near the inner cylinder or (endoscope tube) but in the region $0.47 \le r \le 1.1743$ near outer cylinder quite opposite behavior is observed. Fig. 4 shows the impact of R_m on the axial induced magnetic field hz. The graphical effect displays the axial induced magnetic field hz increases by increasing magnetic Reynolds number R_m.

Figs. (5) to (8) described current density distribution for diverse values of M, N_b, N_t and R_m. It is depicted from Fig. 5 to 7 the current density distribution grows in the portion $1.03 \le r \le 1.4746$, $0.22 \le r \le 0.92$, $0.92 \le r \le 1.4746$ and decays in the portion $0.22 \le r \le 1.02$, $0.921 \le r \le 1.4746$, $0.22 \le r \le 0.91$ with an increase in the values of M, N_b and N_t respectively. One may observe with an increase in the value of N_b current density distribution increases near the inner cylinder, however current density distribution decreases near the inner cylinder by increasing values of M and N_t. It is depicted from Fig. (8) current density distribution increases by increasing values of magnetic Reynolds number. Figs. (9) and (10) are designed to perceive the change of temperature profile for diverse values of N_t and N_b, here temperature profile enhances with the increase of N_t and N_b.

Variation of nanoparticles concentration for various values of N_t (thermophoresis parameter) and N_b (Brownian motion parameter) are depicted in the Figs. (11) and (12). It is observed that nanoparticles concentration falls when the values of N_t are increasing and it enhances when the values of N_b upturns. Peristaltic pumping ($Q > 0$, and $\Delta p > 0$), retrograde pumping ($Q < 0$, and $\Delta p > 0$) and augmented pumping ($Q > 0$, and $\Delta p < 0$) are defined in the Figs. (12) to (14). It is clear pressure rise increases by increasing the value of N_b and decreases by increasing values of N_t in all three regions as shown in Fig. (13) and (14). It is depicted from Fig. 15 pressure rise in the retrograde pumping region increases and decreases in the interval $Q\ \varepsilon[-1.5,-1.1]$, $Q\ \varepsilon[-1,-0.01]$ respectively, whereas pressure rise decreases with the increase in the value of M in peristaltic and augmented pumping region. Friction forces can be seen in the Figs. (16) and (17). One may observe inner and outer friction forces have reverse behavior related to the pressure rise.

Pressure gradient defines in which direction and at what rate pressure changes most rapidly. Figs. (18) – (20) defined the effect of different emerging parameters of our study on the pressure gradient. One explains in the wider part of the annulus $z\varepsilon[0.1, 0.5]$ pressure gradient is comparatively small that is the flow can easily pass without imposition of large pressure gradient where, in the narrowest part of the annulus $z\varepsilon[0.51, 0.9]$ a much larger pressure gradient is essential to preserve the same flux to pass it, especially for the thinnest position on $z = 0.75$. This is in good contract with the physical condition. Also from these figures we can see the impact of M, N_b and N_t on the pressure gradient where the height of dp/dz drops with

enhanced M and N_b and increase as N_t increases.

Trapping is stimulating spectacle of peristaltic wave, which is the expansion of an inside mixing bolus of fluid by protected streamlines. This confined bolus improves pushed forward with the peristaltic wave. To get the possessions of M, N_b and N_t on the trapping, we have prepared Figs. (21) to (23). It is noticed from Figs. 21(a, b, c) that the trapped bolus remains same when the value of M is 0.3 and 0.4 but, the size of the trapped bolus decreases after that, number of the trapped boluses decreases when the value of $M = 1.1$. Figs. 22(a, b, c) represents the effects of N_b on trapping. One comes to know numbers of bolus decreases while bolus become large with greater values of N_b. Figs. 23(a,b,c) discloses that the number of trapped bolus remains same, but the magnitude of trapped bolus slightly shrinks with collective values of N_t.

Concluding remarks

This study inspects the nanoparticles properties on the peristaltic flow of Williamson fluid in an annulus. The leading points of the phenomenon are given as:

1. Induced magnetic field and current density enhances by increasing value of magnetic Reynolds number.
2. It is examined temperature profile upsurges with rise in Brownian motion and thermophoresis parameter.
3. Effects of thermophoresis and Brownian motion parameter on nanoparticle concentration is opposite
4. Friction forces (inner and outer) performed by a different manner related to the pressure rise.
5. Pressure gradient raises as the Hartmann and thermophoresis number increases and lessened by increasing value of Brownian motion parameter.

r	G_r	M	ε	z	q	N_t	B_r	We	ϕ	N_t	w (Absolute Error)
0.97	0.48	1.73	0.2	0.01	0.03	0.89	2.08	0.04	0.02	4.17	0.008508
0.98											0.003719
1											0.000262
0.97	0.49	1.73	0.2	0.01	0.03	0.90	1.9	0.04	0.02	4.17	0.016143
0.98											0.021178
1											0.034813
0.97	0.50	1.73	0.2	0.01	0.03	0.91	1.8	0.04	0.02	4.17	0.000572
0.98											0.005231
1											0.020549

Table 1, Absolute Error for velocity profile with fixed parameters.

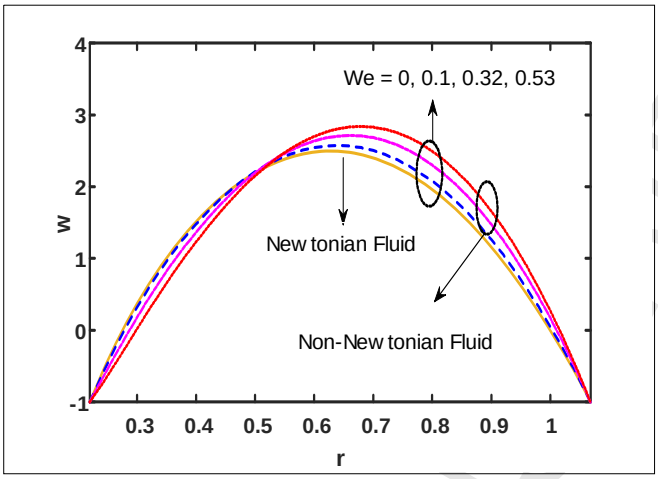

Fig. 1

Fig. 1, Velocity profile for diverse values of We with fixed parameters are $\varepsilon = 0.22,\ N_t = 0.83,$ $N_b = 3.24,\ G_r = 3,\ B_r = 2,\ M = 0.81,\ z = 0.05,\ Q = 0.22.$

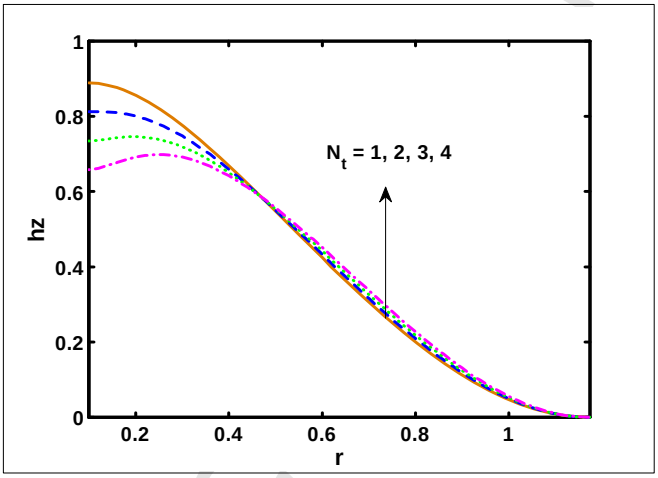

Fig. 2

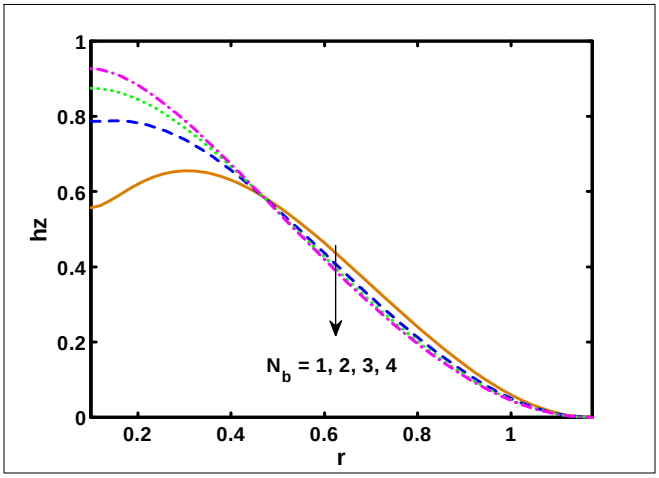

Fig. 3

Fig. 2, Axial induced magnetic field versus r for $N_b = 2.13,\ \phi = 0.18,\ G_r = 0.23,\ B_r = 0.81,$ $z = 0.21,\ \varepsilon = 0.10,\ We = 0.03,\ Q = 0.13,\ M = 0.79,\ R_m = 1.$

Fig. 3, Axial induced magnetic field versus r for $N_t = 2.13,\ \phi = 0.18,\ G_r = 0.23,\ B_r = 0.81,$

$z = 0.21,\ \varepsilon = 0.10,\ We = 0.03,\ Q = 0.13,\ M = 0.79,\ R_m = 1.$

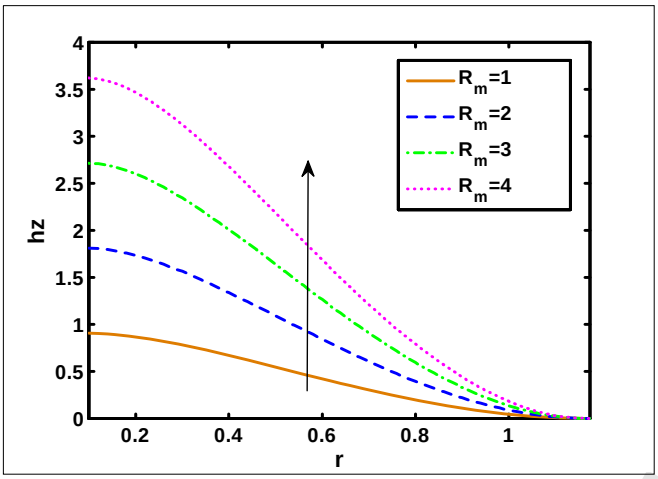

Fig. 4

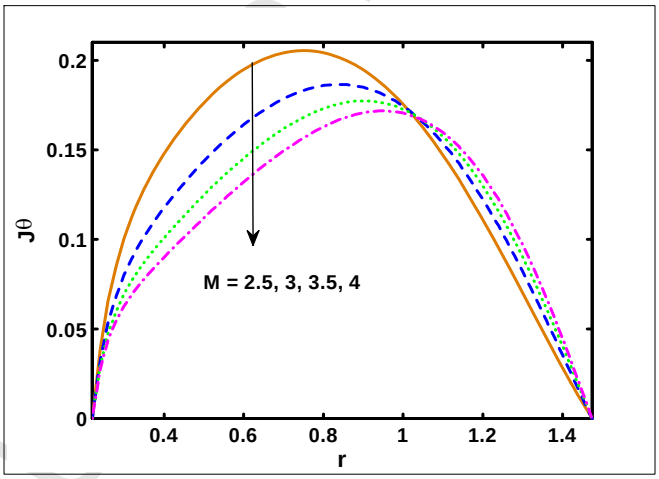

Fig. 5

Fig. 4 Axial induced magnetic field versus r for $\phi = 0.18,\ G_r = 0.23,\ B_r = 0.81,\ z = 0.21,$ $\varepsilon = 0.10,\ We = 0.03, Q = 0.13,\ M = 0.79,\ N_b = 2.13,\ N_t = 0.79.$ **Fig. 5**, Current density distribution versus r for $\phi = 0.49,\ B_r = 0.4,\ G_r = 0.41,\ \varepsilon = 0.22,\ z = 0.21,\ Q = 0.11,$ $R_m = 0.13,\ We = 0.03,\ N_b = 0.79,\ N_t = 0.84.$

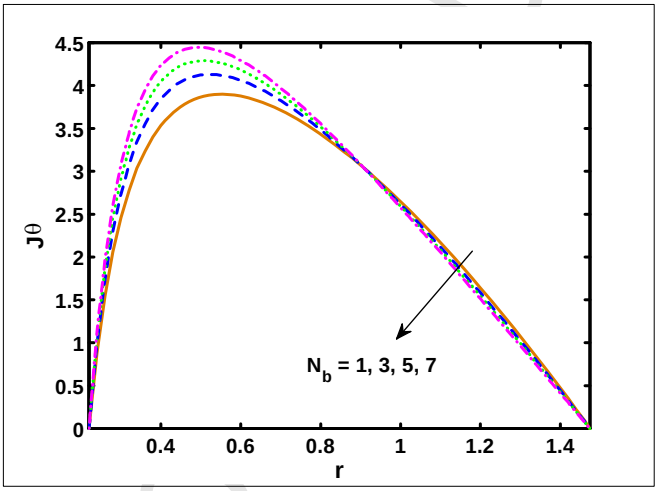

Fig. 6

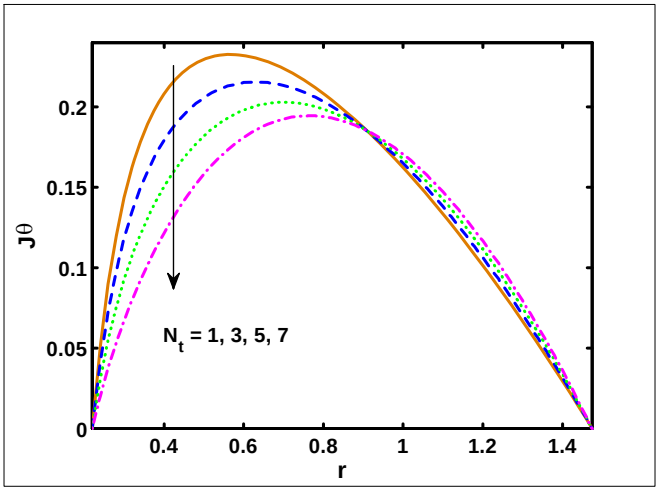

Fig. 7

Fig. 6, Current density distribution versus r for $N_t = 0.79,\ \phi = 0.49,\ B_r = 0.4,\ G_r = 0.41,$

$\varepsilon = 0.22,\ z = 0.21,\ Q = 0.11,\ R_m = 2.13,\ We = 0.03,\ M = 0.84$. **Fig. 7,** $N_b = 0.79,\ \phi = 0.49,$
$B_r = 0.4,\ G_r = 0.41,\ \varepsilon = 0.22,\ z = 0.21,\ Q = 0.11,\ R_m = 0.13,\ We = 0.03.$

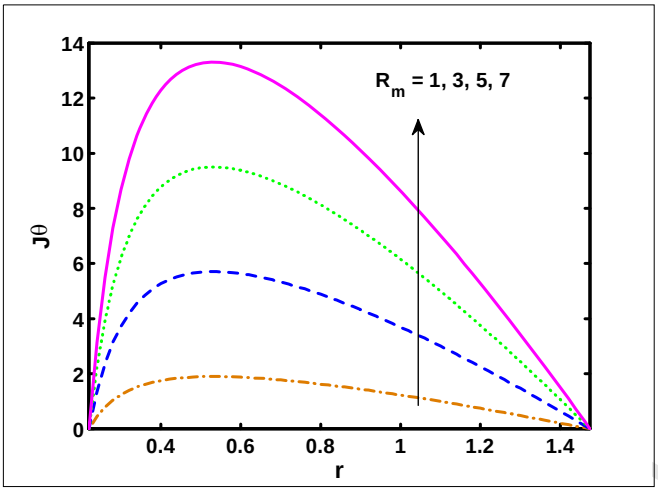

Fig. 8

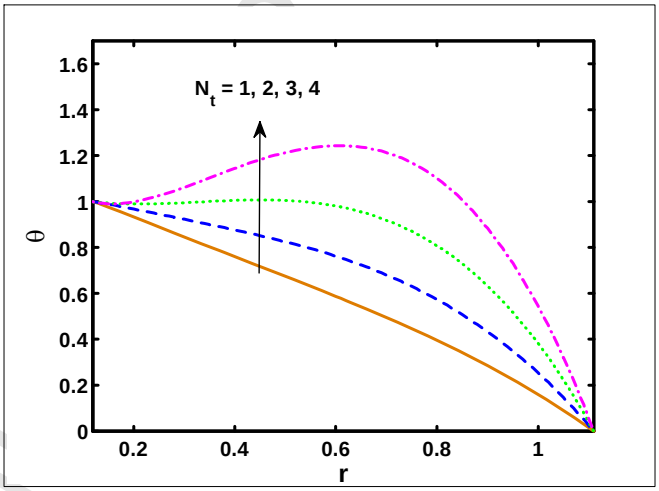

Fig. 9

Fig. 8, Current density distribution versus r for $\phi = 0.49,\ B_r = 0.4,\ G_r = 0.41,\ \varepsilon = 0.22,$ $z = 0.21,\ Q = 0.11,\ We = 0.03,\ N_b = 2.13,\ M = 0.84,\ N_t = 0.79$. **Fig. 9**, Temperature profile versus r for $z = 0.03,\ \varepsilon = 0.12,\ \phi = 0.59, N_b = 1.83.$

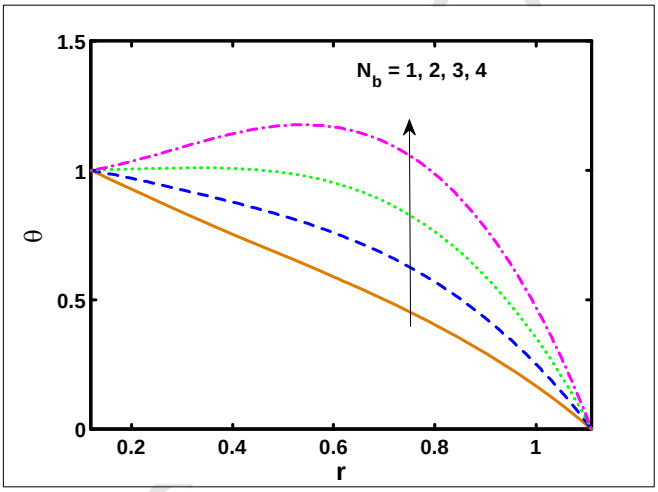

Fig. 10

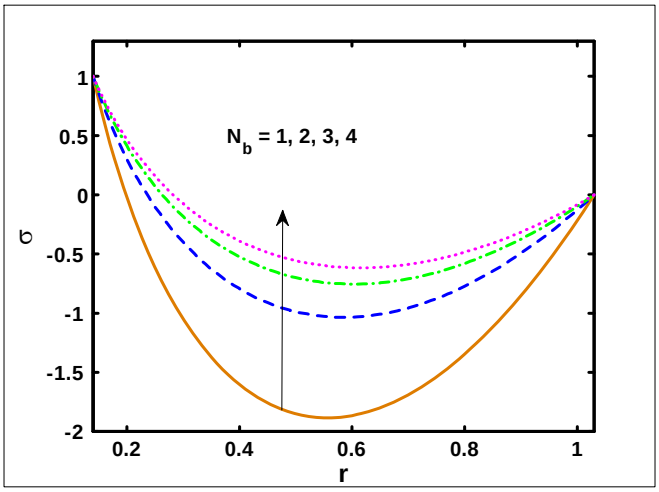

Fig. 11

Fig. 10, Temperature profile versus r for $z = 0.03,\ \varepsilon = 0.12,\ \phi = 0.59, N_t = 1.83$. **Fig. 11,** Nanoparticles concentration versus r for $z = 0.26,\ \phi = 0.03,\ \varepsilon = 0.14,\ N_t = 3.55.$

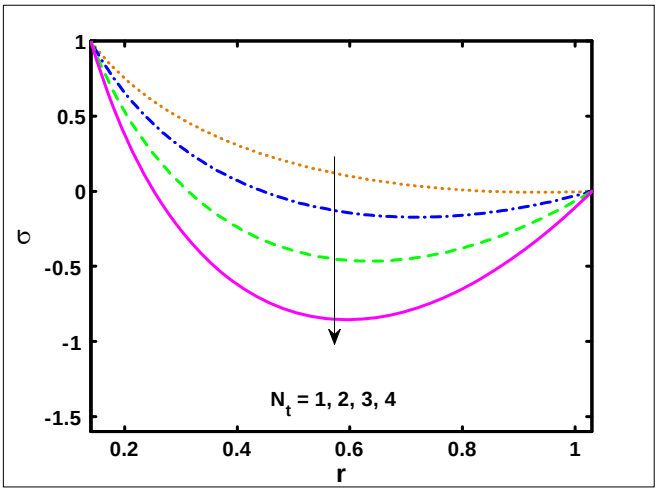

Fig. 12

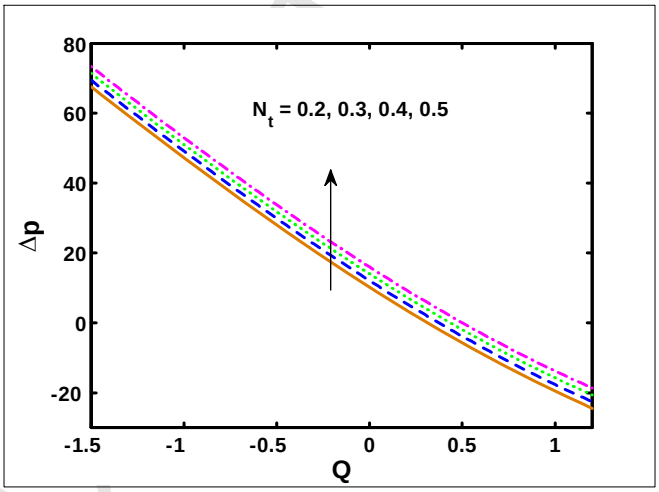

Fig. 13

Fig. 12, Nanoparticles concentration versus r for fixed parameters are $z = 0.26$, $\phi = 0.03$, $\varepsilon = 0.14$, $N_b = 3.55$. **Fig. 13**, Pressure rise versus Q for fixed parameters are $\phi = 0.02$, $B_r = 0.12$, $G_r = 0.13$, $\varepsilon = 0.07$, $We = 0.01$, $N_b = 0.15$, $M = 0.76$.

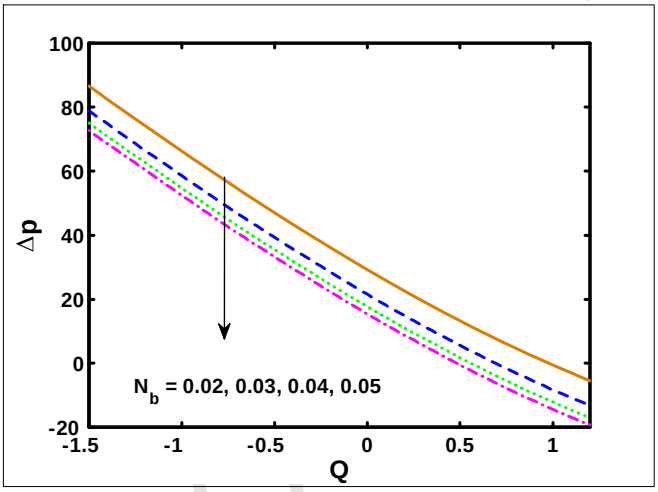

Fig. 14

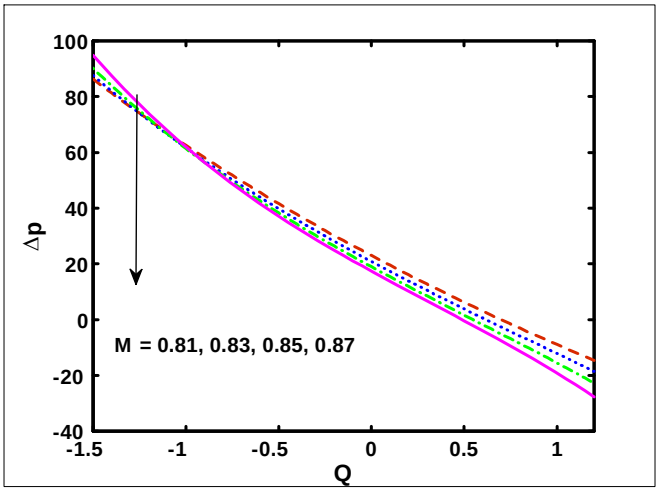

Fig. 15

Fig. 14, Pressure rise against Q for fixed parameters are $M = 0.76$, $\phi = 0.02$, $B_r = 0.12$, $G_r = 0.13$, $\varepsilon = 0.07$, $We = 0.01$, $N_t = 0.15$.

Fig. 15, Pressure rise versus Q for fixed parameters are $\phi = 0.05$, $B_r = 0.12$, $G_r = 0.13$,

$\varepsilon = 0.07,\ We = 0.01,\ N_b = 0.02,\ N_t = 0.15.$

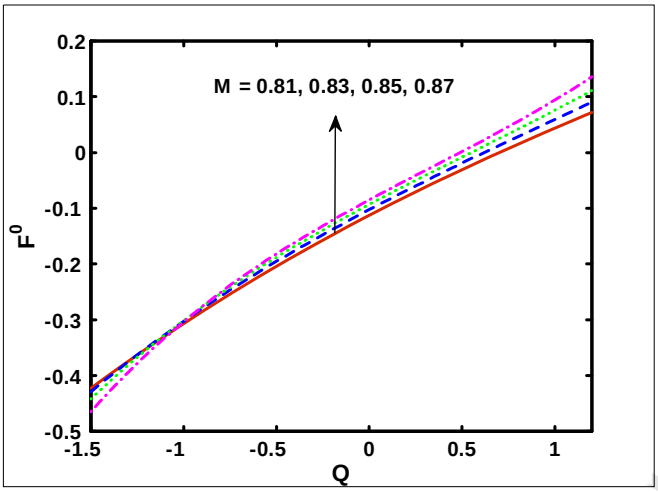

Fig. 16

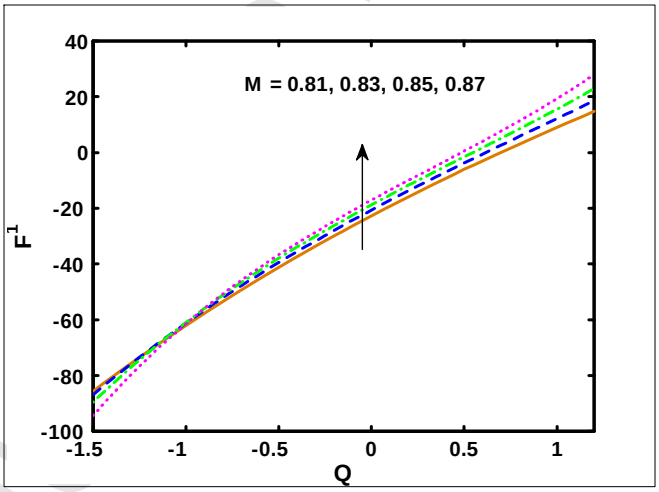

Fig. 17

Fig. 16, (Inner friction forces**)** for $\phi = 0.05,\ B_r = 0.12,\ G_r = 0.13,\ \varepsilon = 0.07,\ We = 0.01,$ $N_b = 0.02,\ N_t = 0.15.$

Fig. 17, (Outer friction forces**)** for $\phi = 0.05,\ B_r = 0.12,\ G_r = 0.13,\ \varepsilon = 0.07,\ We = 0.01,$ $N_b = 0.02,\ N_t = 0.15.$

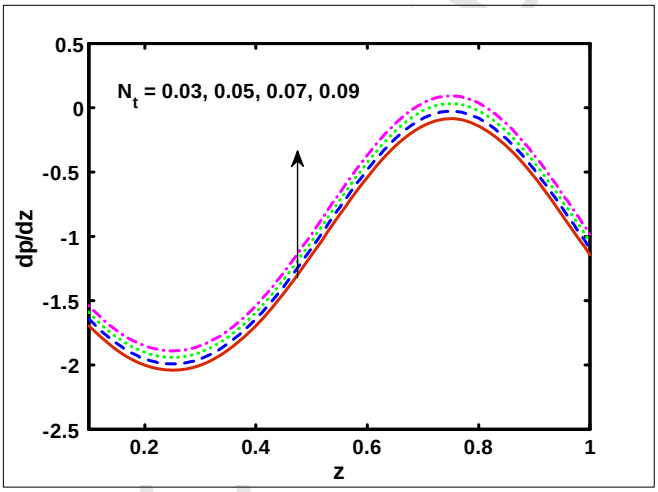

Fig. 18

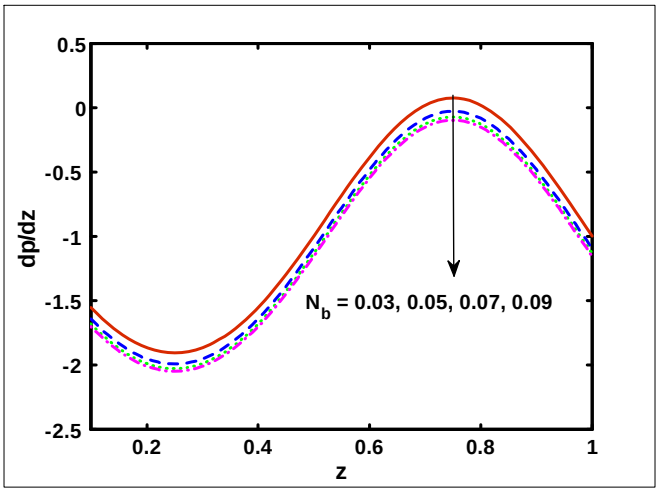

Fig. 19

Fig. (18), Pressure gradient versus z for fixed parameters are $N_b = 0.05,\ \phi = 0.02,\ B_r = 0.12,$

$G_r = 0.13,\ \varepsilon = 0.07,\ We = 0.01,\ M = 1.6,\ Q = 0.03.$

Fig. (19), Pressure gradient versus z for fixed parameters are $N_t = 0.05$, $\phi = 0.02$, $B_r = 0.12$, $G_r = 0.13,\ \varepsilon = 0.07,\ We = 0.01,\ M = 1.6,\ Q = 0.03.$

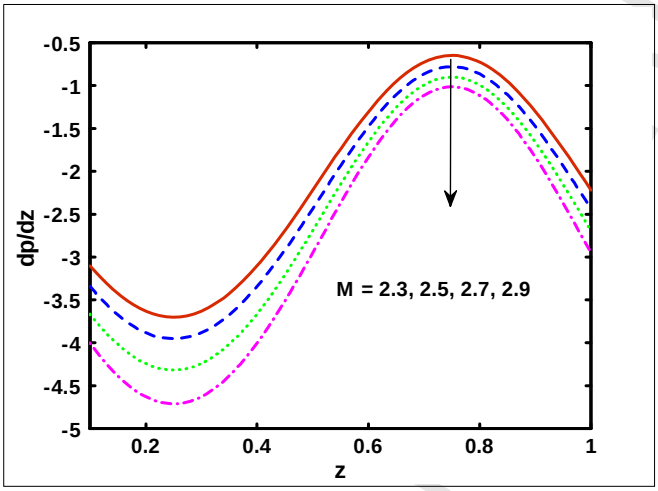

Fig. 20

Fig. (20), Pressure gradient against z for $\phi = 0.02$, $B_r = 0.12$, $G_r = 0.13$, $\varepsilon = 0.07$, $We = 0.01$, $N_t = 0.15$, $N_b = 0.05$ $Q = 0.03$.

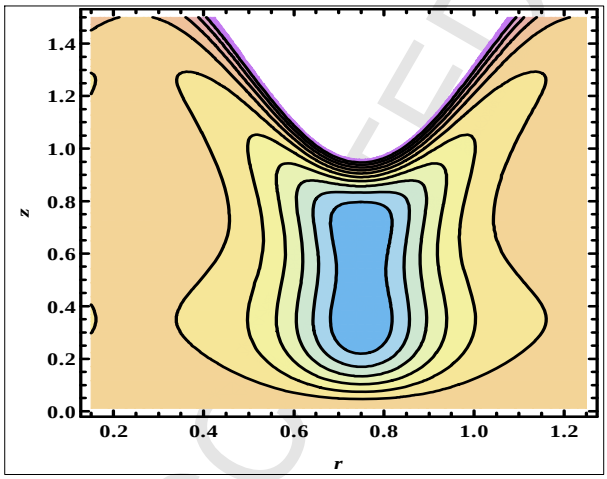

Figure. 21(a)

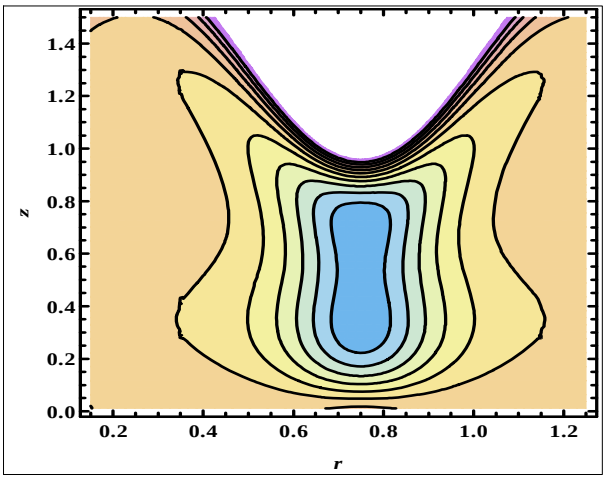

Figure. 21(b)

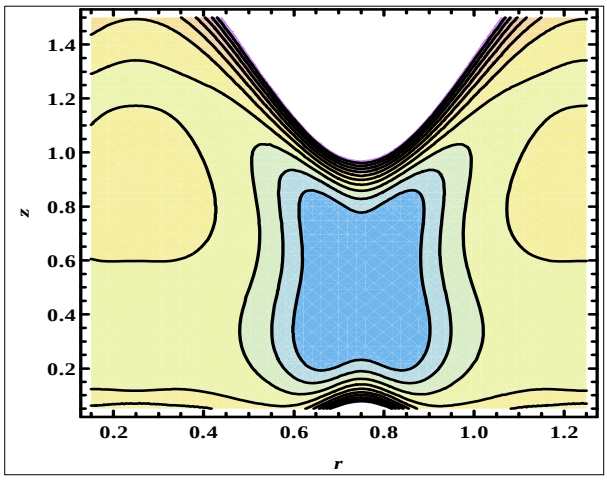

Figure. 21(c)

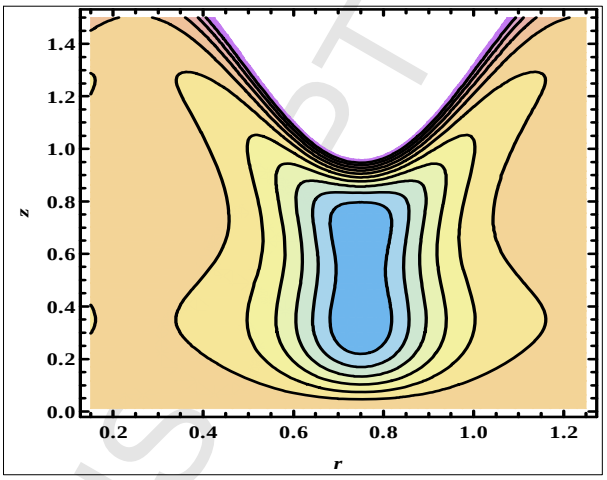

Figure. 22(a)

Fig. (21), Stream lines graphs for diverse values of M, (a, b, c) for $M = 0.3,\ 0.4,\ 1.1$. The other parameter are $\phi = 0.31,\ B_r = 4.79,\ G_r = 2.21,\ \varepsilon = 0.35,\ We = 0.05,\ N_b = 0.23,\ N_t = 5.14,\ Q = 0.13.$

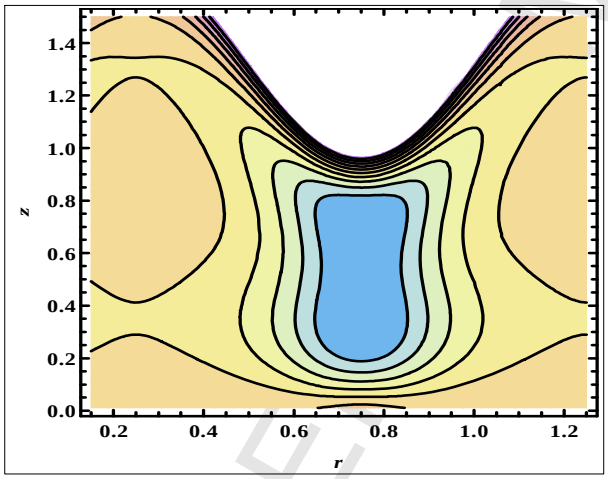

Figure. 22(b)

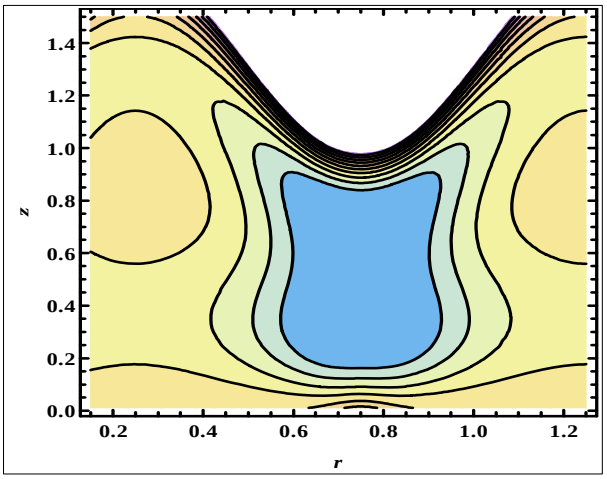

Figure. 22(c)

Fig. (22), Stream lines graphs for diverse values of N_b (a,b,c) for $N_b = 0.23,\ 1.33,\ 2.33$. Other parameters are $\phi = 0.31,\ B_r = 4.79,\ G_r = 2.21,\ \varepsilon = 0.35,\ We = 0.05,\ M = 0.3,\ N_t = 4.14$.

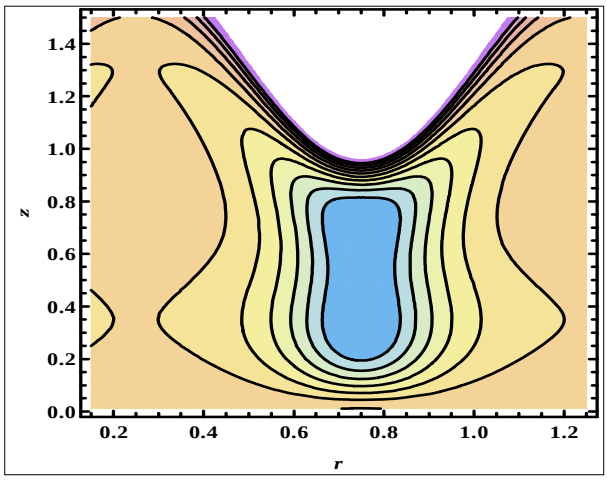

Figure. 23(a)

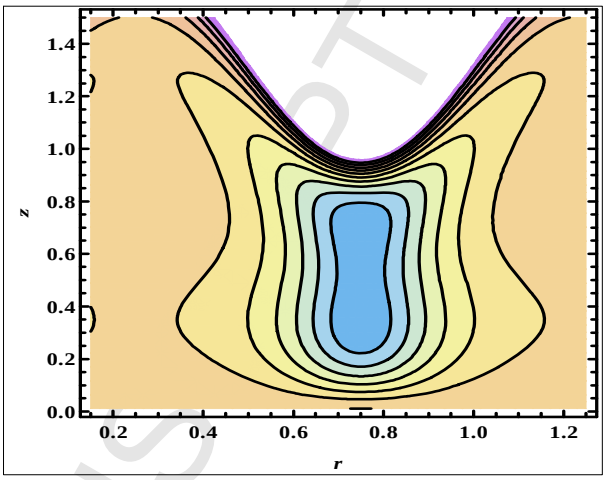

Figure. 23(b)

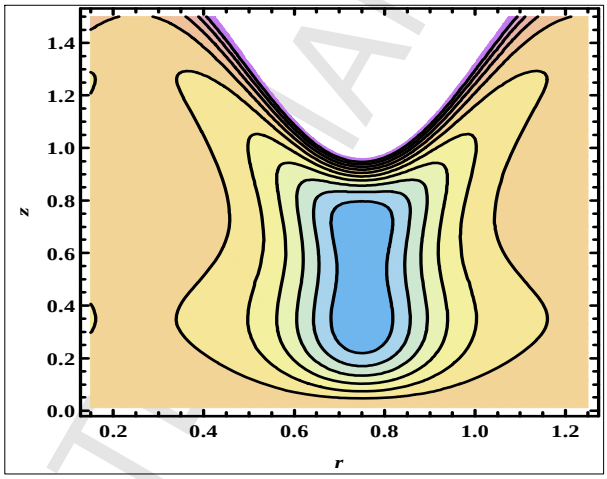

Figure. 23(c)

Fig. (23), Stream lines graphs for diverse values of N_t $(a,\ b,\ c) = 3.14,\ 4.14,\ 5.14$. The other parameter are $B_r = 4.79,\ G_r = 2.21,\ \varepsilon = 0.35,\ We = 0.05,\ M = 0.3,\ N_b = 0.23,\ Q = 0.13.$

Appendix

$$\ell_{11}=\mathrm{r}_1-\mathrm{r}_2,\ \ell_{12}=\frac{\mathrm{r}_2}{\ell_{11}},\ \ell_{13}=N_t+N_b,\ \ell_{13'}=2N_t+N_b,\ \ell_{14}=\ln\mathrm{r}_1-\ln\mathrm{r}_2,$$

$$\ell_{15}=\mathrm{r}_2^2-\mathrm{r}_1^2,\ell_{16}=\frac{-\ell_{13}}{4\ell_{11}^2},\ \ell_{17}=\frac{1}{\ell_{14}}+\frac{\ell_{15}\ell_{16}}{\ell_{14}},\ \ell_{18}=\mathrm{r}_2^2\ln\mathrm{r}_1-\mathrm{r}_1^2\ln\mathrm{r}_2,\ell_{19}=\frac{-\ln\mathrm{r}_2}{\ell_{14}}-\frac{\ell_{16}\ell_{18}}{\ell_{14}},$$

$$\ell_{20}=\ell_{12}+\ell_{19},\ell_{21}=\frac{-\ell_{13}}{N_b\ell_{11}},\ \ell_{22}=\frac{\ell_{12}\ell_{13}}{N_b},\ell_{23}=\frac{-\ell_{21}\ell_{11}}{\ell_{14}},\ \ell_{24}=\mathrm{r}_1\ln\mathrm{r}_2-\mathrm{r}_2\ln\mathrm{r}_1,$$

$$\ell_{25}=\frac{\ell_{21}\ell_{24}}{\ell_{14}}-\ell_{22},\ \ell_{26}=\ell_{22}+\ell_{25},\ell_{27}=\frac{-N_t}{N_b},\ \ell_{28}=\ell_{16}\ell_{27},\ \ell_{29}=\frac{\ell_{27}}{\ell_{11}},\ \ell_{30}=\ell_{17}\ell_{27},$$

$$\ell_{31}=\ell_{20}\ell_{27},\ell_{32}=\frac{\ell_{15}\ell_{28}+\ell_{11}\ell_{29}-\ell_{14}\ell_{30}}{\ell_{14}},\ \ell_{33}=-\frac{\ell_{18}\ell_{28}+\ell_{24}\ell_{29}+\ell_{14}\ell_{31}}{\ell_{14}},\ell_{34}=\ell_{30}+\ell_{32},$$

$$\ell_{35}=\ell_{31}+\ell_{33},\ \ell_{36}=\frac{1}{\ell_{11}}+\ell_{21}-\ell_{29},\ \ell_{37}=\ell_{23}+\ell_{34},\ell_{38}=\ell_{26}-\ell_{12}+\ell_{35},\ \ell_{39}=\frac{-2\ell_{13'}\ell_{16}}{9\ell_{11}},$$

$$\ell_{40}=\frac{-\ell_{13'}}{4\ell_{11}^2}+\frac{N_b\ell_{21}}{4\ell_{11}},\ell_{41}=\frac{-\ell_{13'}\ell_{17}}{\ell_{11}}-\frac{N_b\ell_{23}}{\ell_{11}},\ \ell_{42}=\mathrm{r}_1^3-\mathrm{r}_2^3,\ \ell_{43}=\frac{-\ell_{39}\ell_{42}-\ell_{15}\ell_{40}-\ell_{11}\ell_{41}}{\ell_{14}},$$

$$\ell_{44}=\mathrm{r}_1^3\ln\mathrm{r}_2-\mathrm{r}_2^3\ln\mathrm{r}_1,\ \ell_{45}=\frac{\ell_{39}\ell_{44}+\ell_{18}\ell_{40}+\ell_{24}\ell_{41}}{\ell_{14}},\ \ell_{46}=\ell_{16}-\ell_{40},\ell_{47}=\ell_{17}+\ell_{43},$$

$$\ell_{48}=-\ell_{12}+\ell_{20}+\ell_{45},\ a_{11}=\frac{1}{4-H^2},\ a_{12}=\frac{a_{11}(r_2^{2+H}-r_1^{2+H})}{r_1^{2H}-r_2^{2H}},\ a_{13=}\frac{-a_{11}(r_2^{2+H}r_1^{2H}-r_1^{2+H}r_2^{2H})}{r_1^{2H}-r_2^{2H}},$$

$$a_{14}=2a_{12}a_{13}WeH^2(\frac{dp_0}{dz})^2,a_{15}=12a_{11}^2We(\frac{dp_0}{dz})^2+\frac{G_r+B_r}{r_1-r_2},a_{16}=a_{13}^2WeH^2(\frac{dp_0}{dz})^2$$

$$+2a_{13}^2WeH^3(\frac{dp_0}{dz})^2,$$

$$a_{17}=4a_{11}a_{13}WeH(\frac{dp_0}{dz})^2-4a_{11}a_{13}WeH^2(\frac{dp_0}{dz})^2,a_{18}=-4a_{11}a_{12}WeH(\frac{dp_0}{dz})^2$$

$$-4a_{11}a_{12}WeH^2(\frac{dp_0}{dz})^2,$$

$$a_{19}=a_{12}^2WeH^2(\frac{dp_0}{dz})^2-2a_{12}^2WeH^3(\frac{dp_0}{dz})^2,a_{20}=\frac{(G_r+B_r)r_2}{r_1-r_2},\ a_{21}=\frac{a_{14}}{4-H^2},\ a_{22}=\frac{a_{15}}{9-H^2},$$

$$a_{23}=\frac{a_{16}}{1+3H^2+4H},a_{24}=\frac{a_{17}}{1-2H},a_{25}=\frac{a_{18}}{1+2H},a_{26}=\frac{a_{19}}{1+3H^2-4H},a_{27}=\frac{a_{20}}{1-H^2},$$

$$a_{30}=-2a_{13}a_{28}WeH^2(\frac{dp_0}{dz})-2a_{12}a_{29}WeH^2(\frac{dp_0}{dz})+4a_{12}a_{13}WeH^2((\frac{dp_0}{dz})^2-(\frac{dp_0}{dz})(\frac{dp_1}{dz})),$$

$$a_{31}=-24a_{11}a_{27}We(\frac{dp_0}{dz})+24a_{11}^2We(\frac{dp_0}{dz})^2-24a_{11}^2We(\frac{dp_0}{dz})(\frac{dp_1}{dz})+\frac{G_r}{l_{11}}-B_rl_{21},$$

$$a_{32} = 48a_{11}a_{22}We(\frac{dp_0}{dz}) - G_r l_{16},\ a_{33} = 4a_{13}a_{23}WeH(\frac{dp_0}{dz}) + 14a_{13}a_{23}WeH^2(\frac{dp_0}{dz})$$
$$+12a_{13}a_{23}WeH^3(\frac{dp_0}{dz}),$$
$$a_{34} = 2a_{13}a_{29}WeH^2(\frac{dp_0}{dz}) + 4a_{13}a_{29}WeH^3(\frac{dp_0}{dz}) - 2a_{13}^2WeH^2(\frac{dp_0}{dz})^2 - 4a_{13}^2WeH^3(\frac{dp_0}{dz})^2$$
$$+2a_{13}^2WeH^2(\frac{dp_0}{dz})(\frac{dp_1}{dz}) + 4a_{13}^2WeH^3(\frac{dp_0}{dz})(\frac{dp_1}{dz}),$$
$$a_{35} = -8a_{11}a_{23}WeH(\frac{dp_0}{dz}) - 16a_{11}a_{23}WeH^2(\frac{dp_0}{dz}) - 4a_{13}a_{24}WeH^2(\frac{dp_0}{dz}) + 4a_{13}a_{24}WeH^3(\frac{dp_0}{dz}),$$
$$a_{36} = -4a_{13}a_{21}WeH(\frac{dp_0}{dz}) - 4a_{12}a_{23}WeH(\frac{dp_0}{dz}) - 2a_{13}a_{21}WeH^2(\frac{dp_0}{dz}) - 10a_{12}a_{23}WeH^2(\frac{dp_0}{dz})$$
$$-4a_{12}a_{23}WeH^3(\frac{dp_0}{dz}),$$
$$a_{37} = 4a_{13}a_{27}WeH(\frac{dp_0}{dz}) + 4a_{11}a_{29}WeH(\frac{dp_0}{dz}) - 4a_{13}a_{27}WeH^2(\frac{dp_0}{dz}) - 4a_{11}a_{29}WeH^2(\frac{dp_0}{dz})$$
$$-8a_{11}a_{13}WeH(\frac{dp_0}{dz})^2 + 8a_{11}a_{13}WeH^2(\frac{dp_0}{dz})^2 + 8a_{11}a_{13}WeH(\frac{dp_0}{dz})(\frac{dp_1}{dz})$$
$$-8a_{11}a_{13}WeH^2(\frac{dp_0}{dz})(\frac{dp_1}{dz}),$$
$$a_{38} = (4a_{12}a_{21} + 4a_{13}a_{26})WeH(\frac{dp_0}{dz}) - (2a_{12}a_{21} + 10a_{13}a_{26})WeH^2(\frac{dp_0}{dz}) + 4a_{13}a_{26}WeH^3(\frac{dp_0}{dz}),$$
$$a_{39} = -4a_{12}a_{27}WeH(\frac{dp_0}{dz}) - 4a_{11}a_{28}WeH(\frac{dp_0}{dz}) - 4a_{12}a_{27}WeH^2(\frac{dp_0}{dz}) - 4a_{11}a_{28}WeH^2(\frac{dp_0}{dz})$$
$$+8a_{11}a_{12}WeH(\frac{dp_0}{dz})^2 + 8a_{11}a_{12}WeH^2(\frac{dp_0}{dz})^2 - 8a_{11}a_{12}WeH(\frac{dp_0}{dz})(\frac{dp_1}{dz})$$
$$-8a_{11}a_{12}WeH^2(\frac{dp_0}{dz})(\frac{dp_1}{dz}),$$
$$a_{40} = -8a_{11}a_{24}We(\frac{dp_0}{dz}) - 12a_{13}a_{22}WeH(\frac{dp_0}{dz}) + 12a_{11}a_{24}WeH(\frac{dp_0}{dz}) + 6a_{13}a_{22}WeH^2(\frac{dp_0}{dz})$$
$$-4a_{11}a_{24}WeH^2(\frac{dp_0}{dz}),$$
$$a_{41} = 8a_{11}a_{25}We(\frac{dp_0}{dz}) + 12a_{12}a_{22}WeH(\frac{dp_0}{dz}) - 12a_{11}a_{25}WeH(\frac{dp_0}{dz}) + 6a_{12}a_{22}WeH^2(\frac{dp_0}{dz})$$
$$-4a_{11}a_{25}WeH^2(\frac{dp_0}{dz}),$$

$$a_{42} = 2a_{12}a_{28}WeH^2(\frac{dp_0}{dz}) - 4a_{12}a_{28}WeH^3(\frac{dp_0}{dz}) - 2a_{12}^2WeH^2(\frac{dp_0}{dz})^2 + 4a_{12}^2WeH^3(\frac{dp_0}{dz})^2$$
$$+2a_{12}^2WeH^2(\frac{dp_0}{dz})(\frac{dp_1}{dz}) - 4a_{12}^2WeH^3(\frac{dp_0}{dz})(\frac{dp_1}{dz}),$$
$$a_{43} = 8a_{11}a_{26}WeH(\frac{dp_0}{dz}) - 4a_{12}a_{25}WeH^2(\frac{dp_0}{dz}) - 16a_{11}a_{26}WeH^2(\frac{dp_0}{dz}) - 4a_{12}a_{25}WeH^3(\frac{dp_0}{dz}),$$
$$a_{44} = -4a_{12}a_{26}WeH(\frac{dp_0}{dz}) + 14a_{12}a_{26}WeH^2(\frac{dp_0}{dz}), a_{45} = -G_r l_{17} - B_r l_{23}, a_{46} = -G_r l_{20} - B_r l_{26},$$
$$a_{47} = \frac{a_{30}}{1-H^2},\ a_{48} = \frac{a_{31}}{9-H^2}, a_{49} = \frac{a_{32}}{16-H^2}, a_{50} = \frac{a_{33}}{4+8H^2+12H}, a_{51} = \frac{a_{34}}{1+3H^2+4H},$$
$$a_{52} = \frac{a_{35}}{3H^2}, a_{53} = \frac{a_{36}}{4+4H}, a_{54} = \frac{a_{37}}{1-2H}, a_{55} = \frac{a_{38}}{4-4H}, a_{56} = \frac{a_{39}}{1+2H}, a_{57} = \frac{a_{40}}{4-4H},$$
$$a_{58} = \frac{a_{41}}{4+4H}, a_{59} = \frac{a_{42}}{1+3H^2-4H}, a_{60} = \frac{a_{43}}{3H^2}, a_{61} = \frac{a_{44}}{4+8H^2-12H}, a_{62} = \frac{-a_{45}}{H^2} - \frac{4a_{45}}{H^4},$$
$$a_{63} = \frac{-4a_{45}}{H^4} + \frac{a_{46}}{4-H^2}, a_{66} = (r_1^{-H}r_2^{-H}(-2(4-H^2)r_1^{2+H}r_2^H - 2(4-H^2)r_1^H r_2^{2+H}))/(4(-4+H^2)),$$
$$a_{67} = \frac{r_1^{-H}r_2^{-H}}{4(-4+H^2)}(a_{11}(4-H^2)r_1^{4+H}r_2^H + 4a_{12}(2-H)r_1^{2+2H}r_2^H + a_{11}(-4+H^2)r_1^H r_2^{4+H}$$
$$-4a_{12}(2-H)r_1^H r_2^{2+2H} + 4a_{13}(2+H)(-r_1^H r_2^2 + r_1^2 r_2^H)),$$
$$a_{68} = a_{21}r_1 - \frac{a_{27}r_1^4}{4} + \frac{1}{4}a_{11}\frac{dp_0}{dz}r_1^4 + \frac{a_{22}r_1^5}{5} - \frac{a_{23}r_1^{1-2H}}{1-2H} + \frac{a_{29}r_1^{2-H}}{H-2} + \frac{a_{13}r_1^{2-H}\frac{dp_0}{dz}}{2-H} + \frac{a_{24}r_1^{3-H}}{H-3}$$
$$-\frac{a_{28}r_1^{2+H}}{2+H} + \frac{a_{12}r_1^{2+H}\frac{dp_0}{dz}}{2+H} - \frac{a_{25}r_1^{3+H}}{3+H} - \frac{a_{26}r_1^{1+2H}}{1+2H} - a_{21}r_2 + \frac{a_{27}r_2^4}{4} - \frac{1}{4}a_{11}\frac{dp_0}{dz}r_2^4 - \frac{a_{22}r_2^5}{5}$$
$$+\frac{a_{23}r_2^{1-2H}}{1-2H} + \frac{a_{29}r_2^{2-H}}{2-H} + \frac{a_{13}r_2^{2-H}\frac{dp_0}{dz}}{H-2} - \frac{a_{24}r_2^{3-H}}{H-3} + \frac{a_{28}r_2^{2+H}}{H+2} - \frac{a_{12}r_2^{2+H}\frac{dp_0}{dz}}{H+2} + \frac{a_{25}r_2^{3+H}}{H+3}$$
$$+\frac{a_{26}r_2^{1+2H}}{1+2H},$$
$$a_{69} = -a_{47}r_1 + \frac{a_{62}r_1^4}{16} - \frac{a_{63}r_1^4}{4} - \frac{a_{48}r_1^5}{5} - \frac{a_{49}r_1^6}{6} - \frac{a_{51}r_1^{1-2H}}{1-2H} - \frac{a_{52}r_1^{2-2H}}{2-2H} + \frac{a_{65}r_1^{2-H}}{-2+H} + \frac{a_{54}r_1^{3-H}}{-3+H}$$
$$+\frac{a_{57}r_1^{4-H}}{-4+H} + \frac{a_{50}r_1^{-3H}}{3H} + \frac{a_{53}r_1^{-H}}{H} - \frac{a_{55}r_1^H}{H} - \frac{a_{61}r_1^{3H}}{3H} - \frac{a_{64}r_1^{2+H}}{2+H} - \frac{a_{56}r_1^{3+H}}{3+H} - \frac{a_{58}r_1^{4+H}}{4+H}$$
$$-\frac{a_{59}r_1^{1+2H}}{1+2H} - \frac{a_{60}r_1^{2+2H}}{2+2H} + a_{47}r_2 - \frac{a_{62}r_2^4}{16} + \frac{a_{63}r_2^4}{4} + \frac{a_{48}r_2^5}{5} + \frac{a_{49}r_2^6}{6} + \frac{a_{51}r_2^{1-2H}}{1-2H} + \frac{a_{52}r_2^{2-2H}}{2-2H}$$
$$-\frac{a_{65}r_2^{2-H}}{-2+H} - \frac{a_{54}r_2^{3-H}}{-3+H} - \frac{a_{57}r_2^{4-H}}{-4+H} - \frac{a_{50}r_2^{-3H}}{3H} - \frac{a_{53}r_2^{-H}}{H} + \frac{a_{55}r_2^H}{H} + \frac{a_{61}r_2^{3H}}{3H} + \frac{a_{64}r_2^{2+H}}{2+H}$$
$$+\frac{a_{56}r_2^{3+H}}{3+H} + \frac{a_{58}r_2^{4+H}}{4+H} + \frac{a_{59}r_2^{1+2H}}{1+2H} + \frac{a_{60}r_2^{2+2H}}{2+2H} - \frac{1}{4}a_{62}r_1^4\ln r_1 + \frac{1}{4}a_{62}r_2^4\ln r_2,$$

$$a_{70} = a_{21}r_1 - \frac{a_{27}r_1^4}{4} + \frac{a_{22}r_1^5}{5} - \frac{a_{23}r_1^{1-2H}}{1-2H} + \frac{a_{29}r_1^{2-H}}{H-2} + \frac{a_{24}r_1^{3-H}}{H-3} - \frac{a_{28}r_1^{2+H}}{2+H} - \frac{a_{25}r_1^{3+H}}{3+H}$$
$$- \frac{a_{26}r_1^{1+2H}}{1+2H} - a_{21}r_2 + \frac{a_{27}r_2^4}{4} - \frac{a_{22}r_2^5}{5} + \frac{a_{23}r_2^{1-2H}}{1-2H} + \frac{a_{29}r_2^{2-H}}{2-H} - \frac{a_{24}r_2^{3-H}}{H-3} + \frac{a_{28}r_2^{2+H}}{H+2}$$
$$+ \frac{a_{25}r_2^{3+H}}{H+3} + \frac{a_{26}r_2^{1+2H}}{1+2H}.$$

References

1. T. W. Latham, Fluid motion in a peristaltic pump, MS. Thesis, Massachusetts Institute of Technology, Cambridge, 1966.
2. M. Ealshahed and M. H. Haroun, Peristaltic transport of Johnson-Segalman fluid under effect of a magnetic field, Math. Prob in Eng. 6(2005)663 .
3. Kh. S. Mekheimer, Y. Abd Elmaboud, Peristaltic flow of a couple stress fluid in an annulus; Application of an endoscope, Physica A 387(2008)2403 .
4. M. Kothandapani, S. Srinivas, Peristaltic Transport of a Jeffrey fluid under the effect of magnetic field in an asymmetric channel, Int. J. Non-linear Mechanics $43(2008)915$.
5. S. Nadeem and N. S. Akbar, Series solutions for the peristaltic flow of a Tangent hyperbolic fluid in a uniform inclined tube, Zeitschrift fur Naturforschung $65a(2010)887$.
6. D. Tripathi, O. A. Bég, J. L Curiel-Sosa, Homotopy semi-numerical simulation of peristaltic flow of generalised Oldroyd-B fluids with slip effects, Comput Methods Biomech Biomed Engin $05/2012; DOI : 10.1080/10255842.2012.688109$.
7. R. Ellahi, A. Riaz, S. Nadeem, M. Ali, Peristaltic Flow of Carreau Fluid in a Rectangular Duct through a Porous Medium, Mathl Prob Eng. (2012) doi, org/10.1155/2012/329639.2012.
8. R. Ellahi, A. Riaz, S. Nadeem, Three-dimensional peristaltic flow of Williamson fluid in a rectangular duct, In. J. Phy 87(2013)1275.
9. S. Nadeem, Hina Sadaf, M. Adil Sadiq, Analysis of Nanoparticles on Peristaltic Flow of Prandtl Fluid Model in an Endoscopy, current Nano Science. 11(6)(2015)709.
10. Kh. S. Mekheimer, M. S. Mohamed, Peristaltic transport of a pulsatile flow for a particle-fluid suspension through an annular region: Application of a clot blood model, Int. J. Scien. Engin. Research, 5(11)(2014)845.
11. S. Z. A. Husseny, Y. Abd elmaboud, Kh. S. Mekheimer, The Flow Separation of Peristaltic Transport for Maxwell Fluid between Two Coaxial Tubes, Abst. Appl. Anal. (2014) doi.org/10.1155/2014/269151.
12. Kh. S. Mekheimer, Y. Abd elmaboud, Simultaneous effects of variable viscosity and thermal conductivity on peristaltic flow in a vertical asymmetric channel, Canadian J. Physics, 92(12)(2014)1541.
13. Kh. S Mekheimer, Y. Elmaboud, AI Abdellateef, Hydromagnetic Fow Induced by Sinusoidal Peristaltic Waves through Eccentric Cylinders in a Porous Medium, Walailak J. Sci Tech (WJST) 11(2013)7.
14. Kh. S Mekheimer, Y. Elmaboud, AI Abdellateef, Particulate suspension flow induced by sinusoidal peristaltic waves through eccentric cylinders: Thread Annular, Int. J. Biomath, 06, 1350026 (2013).

15. Kh. S. Mekheimer, A. N. Abdel-Wahab, Net annulus flow of a compressible viscous liquid with peristalsis, J. Aero. Eng, 25(4)(2012)660.
16. R. E. Abo-Elkhair, Kh. S. Mekheimer, A. M. A. Moawad, Cilia walls influence on peristaltically induced motion of magneto-fluid through a porous medium at moderate Reynolds number: Numerical Study, J. Egyp. Math. Soc. 25(2)(2017)238.
17. S. U. S. Choi, Enhancing thermal conductivity of fluids with nanoparticles, in: D.A. Siginer, H.P. Wang (Eds.), Developments and Applications of Non-Newtonian Flows, ASME, New York 66(1995)99.
18. J. Buongiorno, Convective Transport in Nanofluids, J. Heat Transfer (American Society Of Mechanical Engineers) 128(3)(2010)240.
19. S. K. Das, N. Putra, W. Roetzel, Pool boiling of nano-fluids on horizontal narrow tubes, Int J Multiph Flow 29(2003)1237.
20. S. Nadeem, H. Sadaf and A. M. Sadiq, Analysis of Nanoparticles on Peristaltic Flow of Prandtl Fluid Model in an Endoscopy, Current Nanoscience 10(2014)709 .
21. A. V. Kuznetsov and D. A. Nield, Natural convective boundary-layer flow of a nanofluid past a vertical plate, Int. J. Thermal Sci 49(2010)243.
22. W. A. Khan and I. Pop, Boundary-layer flow of a nanofluid past a stretching sheet, Int. J. Heat Mass Tran. 53(2010)2477.
23. S. E. B. Marga, S. J. Palm, C. T. Nguyen, G. Roy and N. Galanis, Heat transfer enhancement by using nanofluids in forced convection flows, Int. J. of Heat and Fluid Flow 26(2005)530.
24. P. Rana and R. Bhargava, Flow and heat transfer of a nanofluid over a nonlinearly stretching sheet: A numerical study, Comm. Nonlinear Sci. Num. Simul *DOI* : 10.1016/*j.cnsns.*2011.05.009.
25. N. S. Akbar and S. Nadeem, Endoscopic effects on the peristaltic flow of a nanofluid, Commun. Theor. Phys. 56(2011)761.
26. R. Ellahi, M. Razab, K. Vafaia, Series solutions of non-Newtonian nanofluids with Reynold's model and Vogel's model by means of the homotopy analysis method, Math and Comp Modl 55(2012)1876.
27. Kh. S. Mekheimer, Effect of the induced magnetic field on peristaltic flow of a couple stress fluid, Phys Lett A 372(2008)4271 .
28. Y. Abd elmaboud, Influence of induced magnetic field on peristaltic flow in an annulus, Commun Nonlinear Sci Numer Simulat 17(2012)685.
29. S. Nadeem, S. Akram, Peristaltic flow of a couple stress fluid under the effect of induced magnetic field in an asymmetric channel, Arch Appl Mech 87(2011)97.
30. R. H. Reddy, A. Kavitha, S. Sreenadh and R. Saravana, Effects of induced magnetic field on peristaltic transport of a carreau fluid in an inclined channel filled with porous material, Int. J. Mech. Mate. Eng. (IJMME) 6(2011)240.
31. Kh. S. Mekheimer, Peristaltic flow of a magneto-micropolar fluid: Effect of induced magnetic field, J App. Math, (2008)570825.
32. J. H. He. Homotopy perturbation technique, Computer Methods in Applied Mechanics and Engineering. 3 (178)(1999)257.
33. J. H. He, A coupling method of a homotopy technique and a perturbation technique for nonlinear problems, Int. J. Non-Linear Mech., 5(1)(2000)37.

34. J. Biazar, M. Eslami, H. Ghazvini, Homotopy perturbation method for systems of partial differential equations, Int. J. Nonlin. Sci. Num. Simul. 8 (3)(2007)411.
35. J. Biazar, H. Ghazvini, M. Eslami, He's homotopy perturbation method for systems of integro-differential equations, Chaos, Solitons and Fractals 3(2009)1253.
36. Z. Odibat, S. Momani, Modified homotopy perturbation method: application to quadratic Riccati differential equation of fractional order, Chaos, Solitons and Fractals 36(1)(2008)167.
37. D. D. Ganji, The application of He's homotopy perturbation method to nonlinear equations arising in heat transfer, Physics Letters A. 355(2006)337.
38. S. Nadeem, S. Akram, Peristaltic flow of a Williamson fluid in an asymmetric channel, Commun. Nonlinear Sci. Numer. Simul. 15(2010)1705.
39. J. H. He, Application of homotopy perturbation method to nonlinear wave equations, Chaos, Solitons & Fractals. 26(2005)695.
40. J. H. He, Homotopy perturbation technique, a new nonlinear analytical technique, Comput. Methods Appl. 135(2003)73.
41. V. P. Rathod and S. K. Asha, Effects of Magnetic Field and an Endoscope on Peristaltic Motion, J. App. Math. 2011(148561).